

ON ENHANCING THE ACCURACY OF EVALUATING GREEN'S FUNCTIONS FOR MULTILAYERED MEDIA IN THE NEAR-FIELD REGION

A. K. Abdelmageed [†] and M. S. Ibrahim

Engineering Mathematics and Physics Department
Faculty of Engineering
Cairo University
Giza 12211, Egypt

Abstract—The discrete complex image method stands as one of the most efficient techniques that is able to represent the Green's functions of multilayered structures accurately in the near- and intermediate-field regions. In order to extend the validity of the method to the far region, the surface waves are extracted. Although the extraction process yields accurate results in the intermediate and far-field regions, erroneous results are observed in the near-field region. In this paper, this problem is treated by extracting the contribution of an additional number of artificial poles. Using this scheme, the discrete complex image method can provide accurate representation of Green's functions in both the near- and far-field regions.

1. INTRODUCTION

The integral equation (IE) has been used extensively as an efficient and rigorous method for the electromagnetic analysis of various multilayered structures; particularly for low and medium sizes. The IE is formulated in terms of Green's functions (GF) which have closed form in the spectral domain [1–3]. The evaluation of the GF in the spatial domain entails the solution of Sommerfeld integrals (SI). These integrals have an oscillatory behavior contributed mainly by the Bessel functions [4]. The presence of branch points and surface-wave poles adds another constraint which makes the numerical solution

[†] He is on leave now to the Public Authority for Applied Education and Training (PAAET), Kuwait. Email:abdelmag@msn.com

of the SI very time consuming. Generally speaking, there is no an analytic solution for the SI. The need of an efficient and fast method to handle these integrals is augmented by the wide applications of the multilayered structures (microwave integrated circuits, microstrip antennas, geophysical prospecting, ... etc). Many methods have been proposed to handle these integrals. One of the most prominent and widely accepted techniques is the discrete complex image method (DCIM) [5–7]. In this method, the quasi-static and contribution of surface-wave poles are extracted first. Hence, the spectral-domain GF is split into three terms: the first term is the quasi-static component, the second is the surface waves, and the third is the remainder part. This remainder part is expanded into a finite series of exponential functions through the use of Prony’s method [8] or generalized pencil-of-function method (GPOF) [9]. To obtain a closed-form solution in the spatial domain, the first and third terms are transformed through the use of the Sommerfeld identity [10], while the second term is transformed via the use of the residue theorem. The near-field region is dominated by the first term and the far-field region is dominated by the second term. The intermediate-field region is mainly contributed by the complex images as expressed by the third term.

The extraction of surface waves has the advantage of extending the validity of the DCIM to the far-field region. The contribution of these surface waves is expressed in terms of Hankel functions. However, the extraction process leads to errors in the near field due to the singularity at the origin related to Hankel functions [11, 12]. To remedy this problem, the authors in [12] introduced a transition point which divides the near- and far-field regions. Hence, the DCIM is applied twice: one with surface-wave extraction which represents the field accurately in the far-field region and the other without surface-wave extraction which represents the field accurately in the near-field region. Alternatively, Abdelmageed and Mohsen [13] have resolved this problem by extracting an artificial pole in addition to each original pole. In the near field, the singularity problem of the Hankel function is removed as the singularity of the artificial pole annihilates the singularity of the original pole. Thereby, the accuracy of the near-field region is preserved. In the far field, the contribution of the artificial pole is highly attenuated leaving only the contribution of the original pole as desired. Teo et al. [14] handled the surface-wave extraction problem adopting a similar approach. They extracted synthetic poles in addition to each original pole. They showed that these synthetic poles and the original one have a better decay rate ($\sim 1/k_\rho^8$) in the spectral domain resulting in good results in the near field.

In this work, we extend the approach adopted in [13]. The

accuracy of the near field is enhanced by extracting more artificial poles. In the spectral domain, the artificial poles and the original one have a better decay rate ($\sim 1/k_\rho^8$) compared with that of [13] ($\sim 1/k_\rho^4$) and similar with that achieved in [14]. In the spatial domain, the surface-wave term has an excellent accuracy in the near field where the singularity of the Hankel function is removed. In the far field, the behavior of the surface-wave term is dominated by the original poles.

2. FORMULATION

A general multilayered medium is shown in Fig. 1. Each layer i is characterized by a relative permittivity ϵ_{ri} , a relative permeability μ_{ri} , and thickness h_i . The bottom layer can be either a dielectric or PEC which is the case illustrated in the figure. A horizontal electric dipole (HED) is assumed to reside on the top layer.

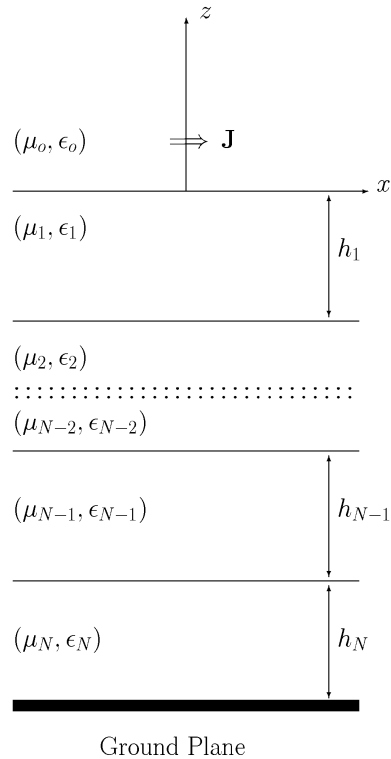


Figure 1. A current source present in a multilayered medium.

The electric field can be represented in terms of the mixed potential integral equation (MPIE) as

$$\mathbf{E}(\mathbf{r}) = -j\omega\mathbf{A}(\mathbf{r}) - \nabla\Phi(\mathbf{r}) \quad (1)$$

where $\mathbf{A}(\mathbf{r})$ and $\Phi(\mathbf{r})$ are the magnetic vector and scalar potentials, respectively. They are defined by

$$\mathbf{A}(\mathbf{r}) = \int d\mathbf{r}' \underline{\underline{\mathbf{G}}}^A(\mathbf{r} | \mathbf{r}') \cdot \mathbf{J}(\mathbf{r}') \quad (2)$$

$$\Phi(\mathbf{r}) = \int d\mathbf{r}' G^q(\mathbf{r} | \mathbf{r}') \nabla' \cdot \mathbf{J}(\mathbf{r}') \quad (3)$$

where $\underline{\underline{\mathbf{G}}}^A$ is the vector potential dyadic Green's function and G^q are the scalar Green's function, and where ∇' operates on the primed (source) coordinates. $\mathbf{J}(\mathbf{r}')$ denotes the electric current density of the source. In this paper, the $e^{j\omega t}$ time convention is assumed and suppressed.

The form of the Green's functions of multilayered media is not unique [15]. Different MPIE formulations have been developed. We adopt here the so-called formulation C developed by Michalski and Zheng [1]. For this formulation, $\underline{\underline{\mathbf{G}}}^A$ can be expressed as

$$\underline{\underline{\mathbf{G}}}^A = \begin{bmatrix} G_{xx}^A & 0 & G_{xz}^A \\ 0 & G_{yy}^A & G_{yz}^A \\ G_{zx}^A & G_{zy}^A & G_{zz}^A \end{bmatrix} \quad (4)$$

In the spectral domain, the components of the $\underline{\underline{\mathbf{G}}}^A$ dyadic and G^q are given in closed form [1]. In the spatial domain, they are expressed in terms of SI. Without losing generality, we consider here the case of an HED which is located in the top layer, as shown in Fig. 1. The typical form of a Green's function component (vector or scalar potential) in the spatial domain can be expressed in terms of SI as

$$G(\rho; z | z') = \frac{1}{4\pi} \int_{-\infty}^{\infty} dk_{\rho} k_{\rho} \tilde{G}(k_{\rho}; z | z') H_0^2(k_{\rho}\varrho) \quad (5)$$

where $\tilde{G}(k_{\rho}; z | z')$ is the spectral-domain counterpart of $G(\rho; z | z')$, and H_0^2 is the zeroth-order Hankel function of the second kind. $\mathbf{r} = (\rho, \phi, z)$ and $\mathbf{r}' = (\rho', \phi', z')$ are the field and source points, respectively, and $\varrho = |\boldsymbol{\rho} - \boldsymbol{\rho}'|$. If the field and source points are in the same layer (top layer), (5) can be written as

$$G(\rho; z | z') = \frac{1}{4\pi} \int_{-\infty}^{\infty} dk_{\rho} \frac{k_{\rho}}{j2k_{zo}} \tilde{F}(k_{\rho}) e^{-jk_{zo}(z+z')} H_0^2(k_{\rho}\varrho) \quad (6)$$

where $k_{zo} = \sqrt{k_o^2 - k_\rho^2}$, and k_o is the wavenumber of the top layer. $\tilde{F}(k_\rho)$ is a spectral function which depends on the physical parameters of the multilayered medium. The first step before applying the DCIM is to extract quasi-static and surface-wave terms [7]:

$$G(\rho; z | z') = G_{qs} + G_{sw} + \frac{1}{4\pi} \int_{-\infty}^{\infty} dk_\rho \frac{k_\rho}{j2k_{zo}} \tilde{F}_r(k_\rho) e^{-jk_{zo}(z+z')} H_0^2(k_\rho \varrho) \quad (7)$$

where G_{qs} and G_{sw} are the quasi-static and surface-wave terms, respectively. Their arguments are omitted for brevity. $\tilde{F}_r(k_\rho)$ is the remainder function which is given as

$$\tilde{F}_r(k_\rho) = \tilde{F}(k_\rho) - \tilde{F}_{qs}(k_\rho) - \tilde{F}_{sw}(k_\rho) \quad (8)$$

where $\tilde{F}_{qs}(k_\rho)$ and $\tilde{F}_{sw}(k_\rho)$ are the spectral-domain quasi-static and surface-wave contributions, respectively. They are given as

$$\tilde{F}_{qs}(k_\rho) = \lim_{k_\rho \rightarrow \infty} \tilde{F}(k_\rho) \quad (9)$$

$$\tilde{F}_{sw}(k_\rho) = \sum_{p=1}^{N_p} \frac{2k_{\rho p} \text{Res}_p}{k_\rho^2 - k_{\rho p}^2} j2k_{zo} e^{jk_{zo}(z+z')} \quad (10)$$

$$\text{Res}_p = \lim_{k_\rho \rightarrow k_{\rho p}} (k_\rho - k_{\rho p}) \left[\frac{e^{-jk_{zo}(z+z')}}{j2k_{zo}} \tilde{F}(k_\rho) \right] \quad (11)$$

where N_p is the number of poles, $k_{\rho p}$'s are the surface-wave poles located in the complex k_ρ -plane, and Res_p 's are their corresponding residues.

The quasi-static term (the first term in (7)) can be obtained analytically using Sommerfeld identity [10]

$$\frac{e^{-jkr}}{4\pi r} = \frac{1}{4\pi} \int_{-\infty}^{\infty} dk_\rho \frac{k_\rho}{j2k_z} e^{-jk_z z} H_0^2(k_\rho \varrho) \quad (12)$$

where $k_z = \sqrt{k^2 - k_\rho^2}$ and $r = \sqrt{\varrho^2 + z^2}$. The surface-wave term (the second term in (7)) can be evaluated using Cauchy's residue theorem:

$$G_{sw} = \frac{1}{4\pi} (-2\pi j) \sum_{p=1}^{N_p} \text{Res}_p H_0^2(k_{\rho p} \varrho) k_{\rho p} \quad (13)$$

The remainder function $\tilde{F}_r(k_\rho)$ can be approximated by a finite series of complex exponentials using Prony's method [8] or the GPOF [9].

$$\tilde{F}_r(k_\rho) = \sum_{l=1}^M a_l e^{-jk_{zo}b_l} \quad (14)$$

Using this representation of $\tilde{F}_r(k_\rho)$, the third term in (7) can be expressed in closed form via the Sommerfeld identity [7]. Thereby, (7) can be written as

$$G(\rho; z | z') = G_{qs} - \frac{j}{2} \sum_{p=1}^{N_p} \text{Res}_p H_0^2(k_{\rho_p} \varrho) k_{\rho_p} + \sum_{l=1}^M a_l \frac{e^{-jk_{o}r_l}}{4\pi r_l} \quad (15)$$

where

$$r_l = \sqrt{\varrho^2 + (z + z' + b_l)^2} \quad (16)$$

Although this expression is valid in principle for all field regions, it suffers from a certain anomaly in the near-field region. The surface-wave term is represented in terms of Hankel functions. The presence of these functions introduces a non-physical singularity when $\varrho \rightarrow 0$ [11, 12]. For $z \neq z'$ (the source and field points are not in the same horizontal plane), the quasi-static term is not singular as $\varrho \rightarrow 0$. However, the Hankel functions have a logarithmic singularity at $\varrho = 0$. The complex images term can not compensate for the singular behavior of the Hankel functions, as the spherical waves of the images fail to represent the logarithmic singularity of these functions. This anomaly has resulted in inaccurate results in the near-field region. However, this problem is eliminated for the special case when $z = z'$ (the source and field points are in the same horizontal plane). In this case, the quasi-static term is singular at $\varrho = 0$, and this singularity dominates over the Hankel functions singularity [16].

The reason of this problem can be explained in the spectral domain [14]. For large k_ρ , the surface-wave term given by (10) decays at a rate of $1/k_\rho^2$ while the complex images needed to represent the remainder function (equation 14) have an exponential decay behavior in the spectral domain. This results in the inability of the complex images to represent the slow decay accurately.

In order to resolve the problem of Hankel function singularity in the near field, we propose to extract a number of artificial poles. Therefore, (10) is modified to include the contribution of additional

three poles.

$$\tilde{F}_{sw}(k_\rho) = \sum_{p=1}^{N_p} S_p(k_\rho) j2k_{z0} e^{jk_{z0}(z+z')} \quad (17)$$

$$S_p(k_\rho) = \frac{2k_{\rho p} \text{Res}_p}{k_\rho^2 - k_{\rho p}^2} + c_1 \frac{2k_{\rho p1} \text{Res}_{p1}}{k_\rho^2 - k_{\rho p1}^2} + c_2 \frac{2k_{\rho p2} \text{Res}_{p2}}{k_\rho^2 - k_{\rho p2}^2} + c_3 \frac{2k_{\rho p3} \text{Res}_{p3}}{k_\rho^2 - k_{\rho p3}^2} \quad (18)$$

where c_i 's are arbitrary constants. The first term belongs to the surface waves extracted at the original pole $k_{\rho p}$. $k_{\rho pi}$'s for $i = 1, 2, 3$ are artificial poles, and Res_{pi} 's are their corresponding residues. The series (18) can be more conveniently represented as

$$S_p(k_\rho) = \sum_{i=0}^3 c_i \frac{2k_{\rho pi} \text{Res}_{pi}}{k_\rho^2 - k_{\rho pi}^2} \quad (19)$$

where $c_0 = 1$, $k_{\rho p0} = k_{\rho p}$ and $\text{Res}_{p0} = \text{Res}_p$. Choosing c_i 's such that

$$c_i k_{\rho pi} \text{Res}_{pi} = d_i k_{\rho p} \text{Res}_p \quad (20)$$

then series (19) can be recast into the form

$$S_p(k_\rho) = 2k_{\rho p} \text{Res}_p \sum_{i=0}^3 d_i \frac{1}{k_\rho^2 - k_{\rho pi}^2} \quad (21)$$

where d_i 's are new arbitrary constants with $d_0 = 1$. The values of d_i 's and $k_{\rho pi}$'s for $i = 1, 2, 3$ are selected such that:

- In the spectral domain, the behavior of $S_p(k_\rho)$ decays at a rate of $1/k_\rho^8$ for large k_ρ .
- In the spatial domain, the behavior of $G_{sw}(\rho)$ renders the true surface-wave behavior in the far-field region, and at the same time does not suffer the singularity problem in the near-field region when $\rho \rightarrow 0$.

With these two conditions kept in consideration, the values of d_i 's and $k_{\rho pi}$'s are given explicitly as

$$d_0 = 1, \quad d_1 = -1, \quad d_2 = -j \left(\frac{k_{\rho p}}{k'_{\rho p}} \right)^2, \quad d_3 = j \left(\frac{k_{\rho p}}{k'_{\rho p}} \right)^2 \quad (22)$$

$$k_{\rho_{p0}} = k_{\rho_p}, \quad k_{\rho_{p1}} = e^{-j\pi/2} k_{\rho_p}, \quad k_{\rho_{p2}} = e^{-j\pi/4} k'_{\rho_p}, \quad k_{\rho_{p3}} = e^{-j3\pi/4} k'_{\rho_p} \quad (23)$$

where $k'_{\rho_p} = \alpha k_{\rho_p} + \beta$. The values of α and β are determined numerically for best results. Using (22) and (23), one can easily verify that $S_p(k_\rho)$ decays with the rate of $1/k_\rho^8$ for large k_ρ . Substituting for $S_p(k_\rho)$, (17) yields

$$\tilde{F}_{sw}(k_\rho) = \left[\sum_{p=1}^{Np} 2k_{\rho_p} \text{Res}_p \sum_{i=0}^3 d_i \frac{1}{k_\rho^2 - k_{\rho_{pi}}^2} \right] j2k_{z0} e^{jk_{z0}(z+z')} \quad (24)$$

Using Cauchy's residue theorem, the surface-wave term G_{sw} takes the form

$$G_{sw} = \frac{1}{4\pi} (-2\pi j) \sum_{p=1}^{Np} \text{Res}_p k_{\rho_p} \sum_{i=0}^3 d_i H_o^2(k_{\rho_{pi}} \varrho) \quad (25)$$

or more explicitly as

$$G_{sw} = -\frac{j}{2} \sum_{p=1}^{Np} \text{Res}_p k_{\rho_p} \left[H_o^2(k_{\rho_p} \varrho) - H_o^2(e^{-j\pi/2} k_{\rho_p} \varrho) \right. \\ \left. - j \left(\frac{k_{\rho_p}}{k'_{\rho_p}} \right)^2 H_o^2(e^{-j\pi/4} k'_{\rho_p} \varrho) + j \left(\frac{k_{\rho_p}}{k'_{\rho_p}} \right)^2 H_o^2(e^{-j3\pi/4} k'_{\rho_p} \varrho) \right] \quad (26)$$

Thus, for each physical pole occurrence the surface-wave term is expressed in terms of a finite series of Hankel functions. The series has four elements. The first element belongs to the surface waves of the original pole, while the other elements belong to the contributions of the artificial poles. Except for the first element, the complex argument of the Hankel functions makes them decay very fast for large ϱ retaining only the contribution of the original pole (the first element). Therefore,

$$\text{For large } \varrho : \quad G_{sw} \longrightarrow -\frac{j}{2} \sum_{p=1}^{Np} \text{Res}_p k_{\rho_p} H_o^2(k_{\rho_p} \varrho) \quad (27)$$

which is the true behavior of surface waves for large ϱ . This asserts that the additional artificial poles do not affect the surface-wave behavior in the far field. To investigate the behavior of (26) in the near field, we use the small argument approximation of the Hankel functions [17]:

$H_0^2(x) \xrightarrow{x \rightarrow 0} \frac{2}{j\pi} \ln x$. Thus,

$$G_{sw} \xrightarrow{\varrho \rightarrow 0} -\frac{1}{\pi} \sum_{p=1}^{Np} \text{Res}_p k_{\rho p} \left[\ln(k_{\rho p} \varrho) - \ln \left(e^{-j\pi/2} k_{\rho p} \varrho \right) - j \left(\frac{k_{\rho p}}{k'_{\rho p}} \right)^2 \ln \left(e^{-j\pi/4} k'_{\rho p} \varrho \right) + j \left(\frac{k_{\rho p}}{k'_{\rho p}} \right)^2 \ln \left(e^{-j3\pi/4} k'_{\rho p} \varrho \right) \right] \quad (28)$$

which simplifies to

$$G_{sw} \xrightarrow{k_{\rho} \rightarrow 0} -\frac{j}{2} \sum_{p=1}^{Np} \text{Res}_p k_{\rho p} \left[1 - j \left(\frac{k_{\rho p}}{k'_{\rho p}} \right)^2 \right] \quad (29)$$

It is obvious that the log singularity of the Hankel function is eliminated and the behavior of the surface-wave term is very smooth in the near-field region.

3. NUMERICAL RESULTS

To demonstrate the accuracy of our proposed method, results are presented for three- and four-layered media of the geometry shown in Fig. 1. For the three-layered medium, layer 0: air, layer 1: $h_1 = 1.0$ mm, $\epsilon_{r1} = 12.6$, layer 2: PEC. For the four-layered medium, layer 0: air, layer 1: $h_1 = 1.5$ mm, $\epsilon_{r1} = 2.1$, layer 2: $h_2 = 0.75$ mm, $\epsilon_{r2} = 12.6$, layer 3: PEC. Results are checked for an HED located at the interface between air and first layer, i.e., $z' = 0$, and for an observation point $z = 1$ mm. The results are validated using direct numerical integration. For brevity, results of only scalar potential G^q are presented. The magnitude of G^q for the three-layered medium are shown in Figs. 2 and 3 for frequency $f = 10, 15$ GHz, respectively. The corresponding results for the four-layered medium are shown in Figs. 4 and 5. For these results, the Green's functions are computed using the DCIM for two different approaches. In the first approach, the original poles of the Green's functions are located and only the surface waves of these original poles are extracted. In the second approach, our proposed method is applied where the contributions of three artificial poles in addition to each original pole are extracted. The values of α and β in (26) are selected for best accuracy: $\alpha = 1.5$, $\beta = 0.5$. From Figs. 2–5, it is readily apparent that extracting only the original surface waves leads to erroneous results in the near field. However, using the proposed method where the contribution of additional three

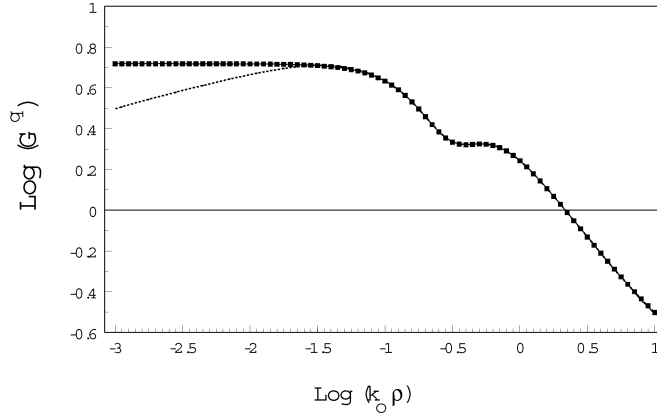


Figure 2. Magnitude of G^q of an HED in a three-layered medium. Layer 0: air, layer 1: $h_1 = 1.0$ mm, $\epsilon_{r1} = 12.6$, layer 2: PEC. $z' = 0$, $z = 1.0$ mm and $f = 10$ GHz. — : Numerical integration and ---- : DCIM with surface-wave extraction. Marks correspond to results obtained by the proposed method.

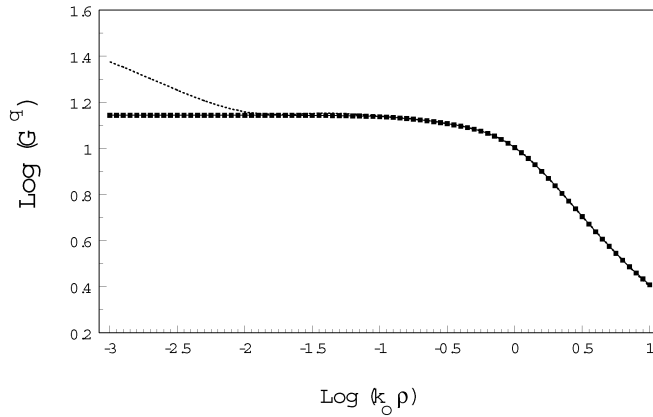


Figure 3. Magnitude of G^q of an HED in a three-layered medium. Layer 0: air, layer 1: $h_1 = 1.0$ mm, $\epsilon_{r1} = 12.6$, layer 2: PEC. $z' = 0$, $z = 1.0$ mm and $f = 15$ GHz. — : Numerical integration and ---- : DCIM with surface-wave extraction. Marks correspond to results obtained by the proposed method.

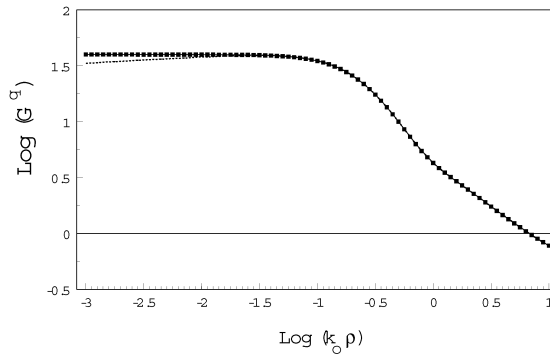


Figure 4. Magnitude of G^q of an HED in a four-layered medium. Layer 0: air, layer 1: $h_1 = 1.5$ mm, $\epsilon_{r1} = 2.1$, layer 2: $h_2 = 0.75$ mm, $\epsilon_{r2} = 12.6$, layer 3: PEC. $z' = 0$, $z = 1.0$ mm and $f = 10$ GHz. — : Numerical integration and ---- : DCIM with surface-wave extraction. Marks correspond to results obtained by the proposed method.

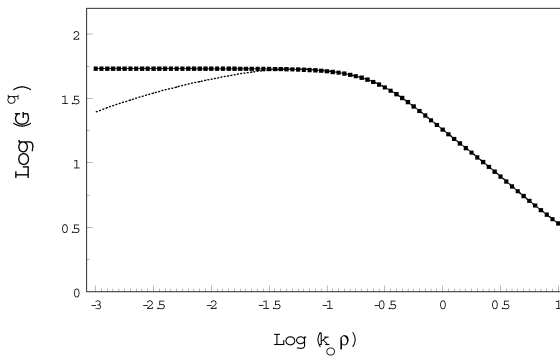


Figure 5. Magnitude of G^q of an HED in a four-layered medium. Layer 0: air, layer 1: $h_1 = 1.5$ mm, $\epsilon_{r1} = 2.1$, layer 2: $h_2 = 0.75$ mm, $\epsilon_{r2} = 12.6$, layer 3: PEC. $z' = 0$, $z = 1.0$ mm and $f = 15$ GHz. — : Numerical integration and ---- : DCIM with surface-wave extraction. Marks correspond to results obtained by the proposed method.

artificial poles are extracted treats this problem and removes the singularity problem which contaminates the results. Obviously, the figures show an excellent agreement of the proposed method with the exact numerical integration in the near-field region as well as other field regions.

To demonstrate the enhanced accuracy achieved by extracting

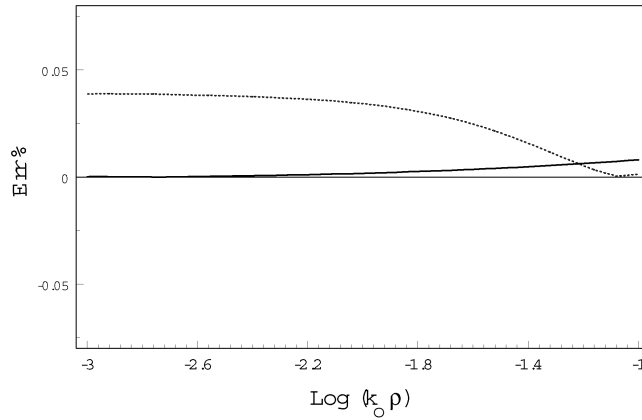


Figure 6. The error occurred in computing the magnitude of G^q of an HED in a four-layered medium. Layer 0: air, layered 1: $h_1 = 1.5$ mm, $\epsilon_{r1} = 2.1$, layered 2: $h_2 = 0.75$ mm, $\epsilon_{r2} = 12.6$, layered 3: PEC. $z' = 0$, $z = 1.0$ mm and $f = 10$ GHz. — : Three artificial poles, ---- : One artificial pole.

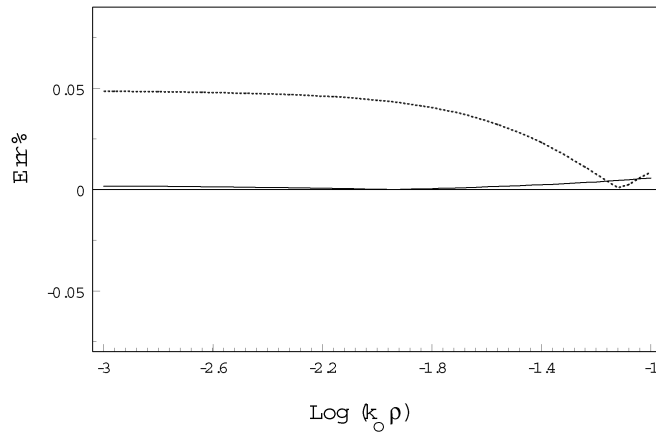


Figure 7. The error occurred in computing the magnitude of G^q of an HED in a four-layered medium. Layer 0: air, layered 1: $h_1 = 1.5$ mm, $\epsilon_{r1} = 2.1$, layered 2: $h_2 = 0.75$ mm, $\epsilon_{r2} = 12.6$, layered 3: PEC. $z' = 0$, $z = 1.0$ mm and $f = 15$ GHz. — : Three artificial poles, ---- : One artificial pole.

three artificial poles, the error occurred in computing Green's functions is calculated using the direct numerical integration as the reference or exact method. Figs. 6 and 7 show the percentage error in the near-field region. The calculations are done for the four-layered medium for the corresponding results shown in Figs. 4 and 5. The results are compared with that of [13], where only one artificial pole is extracted. Observing Figs. 6 and 7, it is evident that the error is much suppressed in the present method. This makes the present method has a much better performance in the near field than that of [13].

4. CONCLUSION

In this work, a new method is proposed for enhancing the accuracy of evaluating Green's functions using the DCIM in the near-field region. Extracting surface waves is known to corrupt the calculated results in the near field due to the singularity at the origin related to Hankel functions. The proposed method handles this deficiency by extracting additional three artificial poles. The new method removes the singularity problem which caused the corruption of results in the near-field region, and at the same time retains the original behavior of the surface waves in the far-field region. The results of the new method is compared with that of the direct numerical integration and an excellent agreement is achieved in all field regions.

REFERENCES

1. Michalski, K. A. and D. Zheng, "Electromagnetic scattering and radiation by surfaces of arbitrary shape in layered media, Part I: Theory," *IEEE Trans. Antennas Propagat.*, Vol. 38, 335–344, 1990.
2. Michalski, K. A. "Formulation of mixed-potential integral equations for arbitrarily shaped microstrip structures with uniaxial substrates," *J. Electromagn. Waves Appl.*, Vol. 7, 799–817, 1993.
3. Oijala, P. Y., M. Taskinen, and J. Sarvas, "Multilayered media Green's functions for MPIE with general electric and magnetic sources by the Hertz potential approach," *Prog. in Electromag. Res.*, Vol. 33, 141–165, 2001.
4. Mosig, J. R., "Integral equation technique," *Numerical Techniques for Microwave and Millimeter-Wave Passive Structures*, T. Itoh (ed.), 133–213, Wiley, New York, 1989.
5. Fang, D. G., J. J. Yang, and G. Y. Delisle, "Discrete image theory

- for horizontal electric dipoles in a multilayered medium,” *IEE Proc., Pt. H*, Vol. 135, 297–303, 1988.
6. Yang, J. J., Y. L. Chow, and D. G. Fang, “Discrete complex images of a three-dimensional dipole above and within a lossy ground,” *IEE Proc., Pt. H*, Vol. 138, 319–326, 1991.
 7. Chow, Y. L., J. J. Yang, D. G. Fang, and G. E. Howard, “A closed-form spatial Green’s function for the thick microstrip substrate,” *IEEE Trans. Microwave Theory Tech.*, Vol. 39, 588–592, 1991.
 8. Marple, S. L., *Digital Spectral Analysis with Applications*, Ch. 11, Prentice-Hall, Englewood Cliffs, New Jersey, 1987.
 9. Hua, Y. and T. K. Sarkar, “Generalized pencil-of-function method for extracting poles of an EM system from its transient response,” *IEEE Trans. Antennas Propagat.*, Vol. 37, 229–234, 1989.
 10. Chew, W. C., *Waves and Fields in Inhomogeneous Media*, Ch. 2, Van Nostrand Reinhold, New York, 1990.
 11. Hojjat, N., S. Safavi-Naeini, and Y. L. Chow, “Numerical computation of complex image Green’s functions for multilayer dielectric media: Near-field zone and the interface region,” *IEE Proc. Microwaves, Antennas and Propagat.*, Vol. 145, 449–454, 1998.
 12. Ling, F. and J. M. Jin, “Discrete complex image method for Green’s functions of general multilayer media,” *IEEE Microw. Guided Wave Lett.*, Vol. 10, 400–402, 2000.
 13. Abdelmageed, A. K. and A. Mohsen, “An accurate computation of Green’s functions for multilayered media in the near-field region,” *Microwave & Opt. Technol. Lett.*, Vol. 29, 130–131, 2001.
 14. Teo, S. A., S. T. Chew, and M. S. Leong, “Error analysis of the discrete complex image method and pole extraction,” *IEEE Trans. Microwave Theory Tech.*, Vol. 51, 406–413, 2003.
 15. Michalski, K. A., “On the scalar potential of a point charge associated with a time-harmonic dipole in a layered medium,” *IEEE Trans. Antennas Propagat.*, Vol. 35, 1299–1301, 1987.
 16. Boix, R. R., F. Mesa, and F. Medina, “Application of total least squares to the derivation of closed-form Green’s functions for planar layered media,” *IEEE Trans. Microwave Theory Tech.*, Vol. 55, 268–280, 2007.
 17. Abramowitz, M. and I. Stegun (eds.), *Handbook of Mathematical Functions*, Ch. 9, Dover, New York, 1970.